

# Effect of deep gain layer and Carbon infusion on LGAD radiation hardness

R Padilla, C. Labitan, Z. Galloway, C. Gee, S. M. Mazza<sup>1</sup>,  
 F. McKinney-Martinez, H. F.-W. Sadrozinski, A. Seiden, B. Schumm,  
 M. Wilder, Y. Zhao, H. Ren, Y. Jin, M. Lockerby,  
 V. Cindro, G. Kramberger, I. Mandiz, M. Mikuz, M. Zavrtanik,  
 R. Arcidiacono, N. Cartiglia, M. Ferrero, M. Mandurrino, V. Sola, A. Staiano

## Abstract

The properties of 50  $\mu\text{m}$  thick Low Gain Avalanche Diode (LGAD) detectors manufactured by Hamamatsu photonics (HPK) and Fondazione Bruno Kessler (FBK) were tested before and after irradiation with 1 MeV neutrons. Their performance were measured in charge collection studies using  $\beta$ -particles from a  $^{90}\text{Sr}$  source and in capacitance-voltage scans (C-V) to determine the bias to deplete the gain layer. Carbon infusion to the gain layer of the sensors was tested by FBK in the UFSD3 production. HPK instead produced LGADs with a very thin, highly doped and deep multiplication layer. The sensors were exposed to a neutron fluence from  $4 \times 10^{14} \text{ n}_{\text{eq}}/\text{cm}^2$  to  $4 \times 10^{15} \text{ n}_{\text{eq}}/\text{cm}^2$ . The collected charge and the timing resolution were measured as a function of bias voltage at -30C, furthermore the profile of the capacitance over voltage of the sensors was measured.

## 1 Introduction

Low Gain Avalanche Detectors (LGADs) are thin (20 to 60  $\mu\text{m}$ ) n-on-p silicon sensors with modest internal gain (typically 5 to 50) and exceptional time resolution (17 ps to 50 ps) [1, 2, 3]. LGADs were first developed by the Centro Nacional de Microelectrónica (CNM) Barcelona, in part as a RD50 Common Project [4]. The internal gain is due to a highly doped p+ region (called multiplication or gain layer) just below the n-type implants of the electrodes. The multiplication layer is up to a few microns thick, while the rest of the active area is referred to as the bulk. Thanks to their extraordinary properties LGADs establish a new paradigm for space-time particle tracking [5].

The first application of LGADs are planned for the High Luminosity LHC (HL-LHC [6]), where the extreme pileup conditions will lower the efficiency for tracking and vertexing of the inner tracking detector in the region close to the beam-pipe. Therefore, to maintain the performance, LGAD based timing layers are foreseen in the forward region of both the ATLAS and the CMS experiments. The two projects are called respectively the High Granularity Timing Detector (HGTD) [7] and the End-cap Timing Layer (ETL) [8]. At HL-LHC, LGADs would be of moderate segmentation (1.3 mm x 1.3 mm) and will have to face challenging radiation requirements, with fluences up to few  $1 \times 10^{15} \text{ n}_{\text{eq}}/\text{cm}^2$  and doses up to few MGy.

LGADs from several vendors have been tested extensively during the last few years. LGAD sensors have been proven to be able to reach a time resolution, before radiation damage, between 17 ps and 50 ps depending on thickness and doping profile. These measurements are in agreement with the simulation program Weightfield2 (WF2) [9]. Previous studies on LGAD sensors from different vendors are reported in [10, 11, 12, 13, 14]. In all cited cases, both the timing resolution and the gain deteriorate with radiation damage due to the acceptor removal mechanism [15], which reduces the effective doping concentration in the gain layer. In the following sections it will be shown that the performance loss from radiation damage can be partly recovered by increasing the bias voltage applied to the sensor and that optimized sensor design can increase the recovery of performance after irradiation.

<sup>1</sup>Corresponding author, simazza@ucsc.edu

Manufacturer	Type	Active Thickness	Physical Thickness	$V_{FD}$	$V_{BD}$	Carbon
HPK	HPK-3.1	50 $\mu\text{m}$	300 $\mu\text{m}$	50 V	250 V	no
HPK	HPK-3.2	50 $\mu\text{m}$	300 $\mu\text{m}$	70 V	120 V	no
FBK	FBK3+C	55 $\mu\text{m}$	500 $\mu\text{m}$	25 V	400 V	yes
FBK	FBK3noC	55 $\mu\text{m}$	500 $\mu\text{m}$	25 V	400 V	no

Table 1: Parameters of the detectors under study (at +20C), including Full Depletion Voltage ( $V_{FD}$ ) and Breakdown Voltage ( $V_{BD}$ )

## 2 Sensor types and electrical properties

The four sensor types under study include two types by HPK, from a shared ATLAS-CMS LGAD prototype production, and two types by FBK from the INFN-funded production run called UFSD3. Tab. 1 shows the basic parameters of the four sensor types. The geometry of the sensors tested is either single pads (HPK only) or 2x2 arrays (HPK and FBK), the pad dimension in all types is 1.3 mmx1.3 mm.

Both types of HPK sensors have a thin, highly-doped, deep multiplication layer, with HPK-3.2 having the deepest multiplication layer. In a deeper gain layer, such as that of HPK-3.2, the recovery of the gain due to an increase of the bias voltage is more pronounced since it is acting on a longer distance. This design, therefore, is not more radiation resistance because the acceptor removal mechanism is slower, but because the bias voltage has stronger recovery capability.

The two FBK sensor types are identical with the exception of FBK3+C having carbon added to the gain layer. Carbon was proven to increase the radiation hardness of LGADs because part of the Si interstitials responsible for Boron removal in the multiplication layer are de-activated by carbon capture. However, since carbon is electrically inactive, its addition does not affect the sensor performance before irradiation. This effect was already observed in the past FBK production FBK-UFSD2 [10, 11].

Basic electrical measurements on the sensors were done using a probe station equipped with needle contacts. The current-voltage (I-V) and the capacitance-voltage (C-V) scans were performed for all detectors. The I-V measurements are used to evaluate the Breakdown Voltage ( $V_{BD}$ ) in Tab. 1, while the C-V are used to evaluate the Full Depletion Voltage ( $V_{FD}$ ). The C-V measurements were taken at 10 kHz for unirradiated sensors and at 1 kHz for irradiated sensors. The measured C-V curves for all sensor types before irradiation are shown in Fig. 1 (left); the curves exhibit a strong fall-off at the bias where the gain layer depletes after which the C-V curve quickly reaches the saturation value revealing a lightly doped bulk. The initial capacitance at low voltage (e.g. the capacitance value around 10 V for all sensor types) is an indication of the depth of the gain layer; assuming the area is the same a lower capacitance is an indication of a deeper gain layer.

Studying the  $1/C^2$  curve, Fig. 1 (right), three sections of the curve are common to all sensor types: a first flat section which corresponds to the depletion of the gain layer, then a fast rising section which corresponds to the depletion of the bulk and finally a flat constant part corresponding to the fully depleted sensor. The intercept of the extensions of the fast rising section of the curve and the first flat section of the curve is called the “foot” ( $V_{GL}$ ) and is proportional to the doping density in the multiplication layer multiplied by its depth. The slope of the fast rising part of the curve is proportional to the doping density of the bulk.

Additional information can be extracted from the  $1/C^2$  curve, assuming a similar doping for the gain layer of all types. It can be seen that the gain layer of FBK3+C and FBK3noC sensors have the same profile and have the lowest  $V_{GL}$  (around 25 V) which correspond to a shallow gain layer. Then HPK-3.1 has a higher  $V_{GL}$  (around 40 V) corresponding to a deeper gain layer,

finally HPK-3.2 has the highest  $V_{GL}$  (around 55 V) corresponding to the deepest layer.

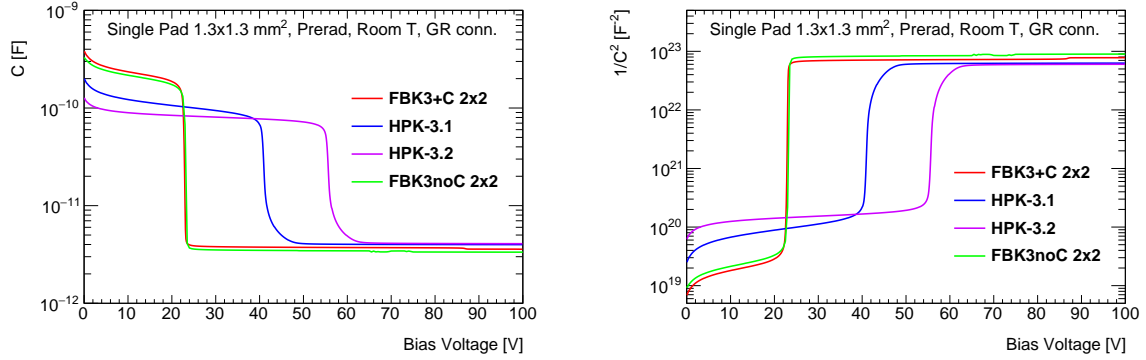


Figure 1: C-V scan (Left) and  $1/C^2$  distribution (right) of HPK and FBK3 sensors before irradiation.

### 3 Neutron irradiation at JSI

The UFSD were irradiated without bias in the JSI research reactor of TRIGA type in Ljubljana, which has been used successfully in the past decades to support the development of radiation hard sensors [16] with fluences between  $4 \times 10^{14} \text{ n}_{eq}/\text{cm}^2$  to  $4 \times 10^{15} \text{ n}_{eq}/\text{cm}^2$ . The neutron spectrum and flux are well known and the fluence is quoted in 1 MeV equivalent neutrons per  $\text{cm}^2$  ( $n_{eq}/\text{cm}^2$ ).

After irradiation, the devices were annealed for 80 min at 60 C. Afterward the devices were kept in cold storage at -20 C to reduce further annealing.

### 4 Beta-scope setup and data analysis

The charge collection experimental setup at UCSC relies on a 90Sr beta-source, with a setup described in detail in [10, 12, 13]. The device under test (DUT) is mounted on a fast analog electronic board (up to 2 GHz bandwidth) digitized by a GHz bandwidth digital scope. The trigger, which acts as a time reference, is also mounted on a fast electronic board, and it is provided by a second HPK UFSD with time resolution of 17ps. The electronic boards are mounted on a frame that aligns DUT and trigger to the 90Sr source. The system is housed in a climate chamber allowing operations of irradiated sensors at temperatures down to -30C in a dry environment. Sensors before irradiation were tested both at 20C and -30C.

The digital oscilloscope records the full waveform of both trigger and DUT in each event, so the complete event information is available for offline analysis. The data analysis follows the steps listed in [10, 12, 13] and proceeds as follows. The first step is a selection: for a valid trigger pulse, the signal amplitude Pmax of the DUT UFSD should not be saturated by either the scope or the read-out chain. To eliminate the contributions from non-gain events or noise, the time of the pulse maximum has to fall into a window of 1 ns centered on the trigger pulse. The selected event waveforms are then analyzed to calculate the distribution of the pulse maximum, the collected charge, the gain, the rise and fall time and the time resolution.

For the calculation of the time resolution a Constant Fraction Discriminator (CFD) of 50% is used to evaluate the time of arrival for the DUT and a CFD of 20% for the time of arrival of the trigger. Then the distribution of the time differences between DUT and trigger is built the  $\sigma$  of a gaussian fit to the distribution is taken as the time resolution. The time resolution of the DUT is then calculated by removing in quadrature the time resolution of the trigger, which is known<sup>2</sup>.

<sup>2</sup>The time resolution for the trigger UFSD was measured by pairing two identical UFSDs

The area of the pulse is evaluated for the DUT, subtracting the subsequent undershoot, then it is divided by the trans-impedence of the amplifier system ( $4700\ \Omega$ ) to calculate the collected charge. The gain of the DUT LGAD is calculated dividing the collected charge by the collected charge of a same thickness PiN diode with no gain. The PiN diode charge is calculated with the Weightfield2 [9] simulation software tuned with measurements of irradiated PiN diodes as explained with more detail in [10].

## 5 Performance of unirradiated and irradiated sensors

Sensors were tested with the Sr90 setup described in the previous section before and after irradiation with neutrons at JSI. The relevant measured parameters are the gain, which is proportional to the collected charge, and the time resolution. As seen in Fig. 2 for HPK-3.2, HPK-3.1 and FBK3+C the gain decreases with the fluence but can be restored by increasing the bias voltage applied. However it was not possible to recover in this way a substantial gain at fluences above  $3 \times 10^{15}\ \text{n}_{\text{eq}}/\text{cm}^2$ .

The performance of these sensors can be summarized as follows. HPK-3.2 shows a very high gain before irradiation and up to  $3 \times 10^{15}\ \text{n}_{\text{eq}}/\text{cm}^2$  it can still reach a gain of 8. HPK-3.1 shows a similar performance (although at higher voltages) before irradiation but can reach a gain of 8 only up to  $1.5 \times 10^{15}\ \text{n}_{\text{eq}}/\text{cm}^2$ . FBK3+C has a lower overall gain but it can maintain it up to a fluence of  $3 \times 10^{15}\ \text{n}_{\text{eq}}/\text{cm}^2$ . FBK3 sensors performance is not shown before irradiation because of an issue in the production that causes excessive noise in new sensors, this issue is already solved in the new production FBK3.1. Finally, no sensor shows gain over 4 after a fluence of  $4 \times 10^{15}\ \text{n}_{\text{eq}}/\text{cm}^2$ .

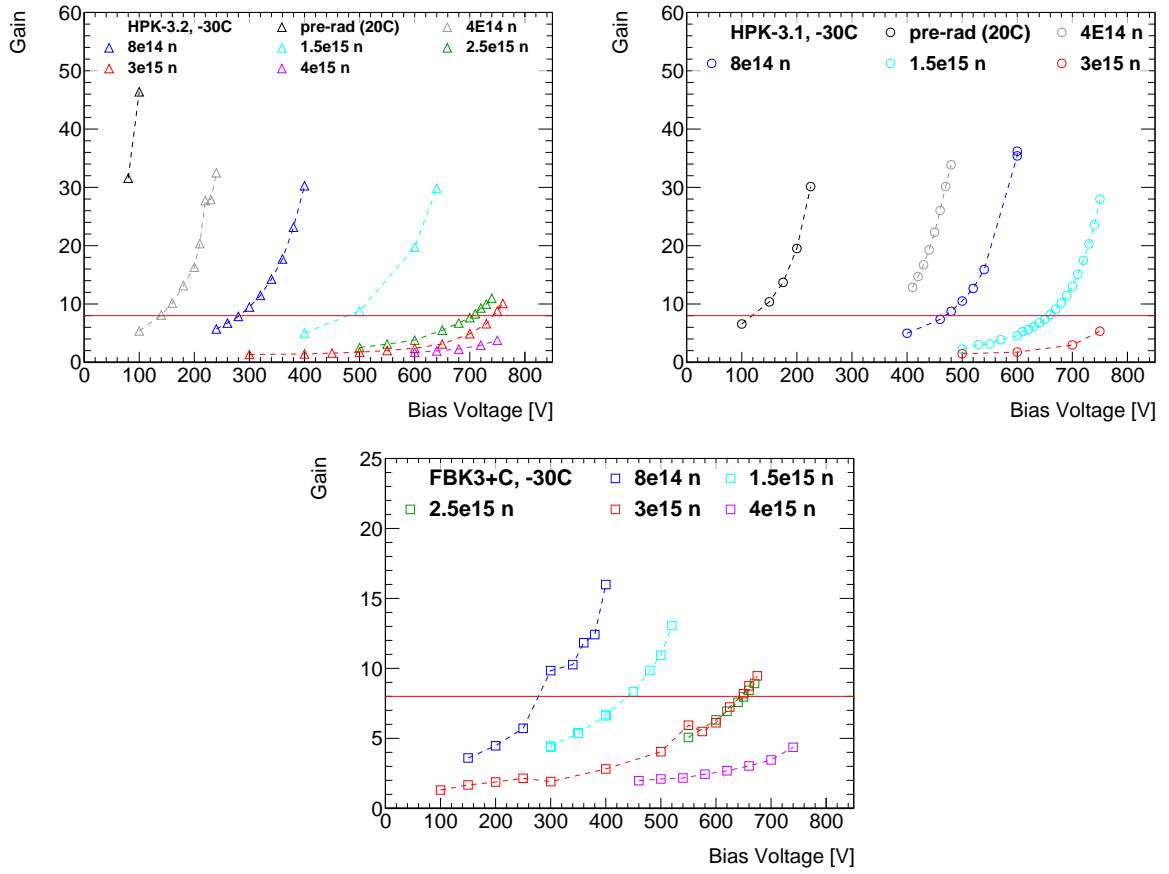


Figure 2: Gain as a function of bias voltage for HPK-3.2 (top-left), HPK-3.1 (top-right) and FBK3+C (bottom) sensors. The red horizontal line is for comparison purposes and represents a gain of 8. The plots for HPK-3.2/HPK-3.1 have a different vertical scale than for FBK3+C.

In Fig. 3 (left) the direct comparison of HPK-3.1 and HPK-3.2 is shown. The two types of HPK sensors show different behavior before irradiation, with HPK-3.2 showing high gain even at a low voltage. After irradiation however HPK-3.1 maintains reasonable gain only up to  $1.5 \times 10^{15} \text{ n}_{\text{eq}}/\text{cm}^2$  while HPK-3.2 still performs well until  $3 \times 10^{15} \text{ n}_{\text{eq}}/\text{cm}^2$ , so it has roughly twice the reach in fluence.

In Fig. 3 (right) is shown how FBK3+C and FBK3noC sensors, which have the same structure before irradiation (Fig. 1), have a very different behavior at the fluence of  $2.5 \times 10^{15} \text{ n}_{\text{eq}}/\text{cm}^2$ . The sensor with Carbon (FBK3+C) still maintains a reasonable gain while the sensor without carbon (FBK3noC) has a gain that is reduced drastically.

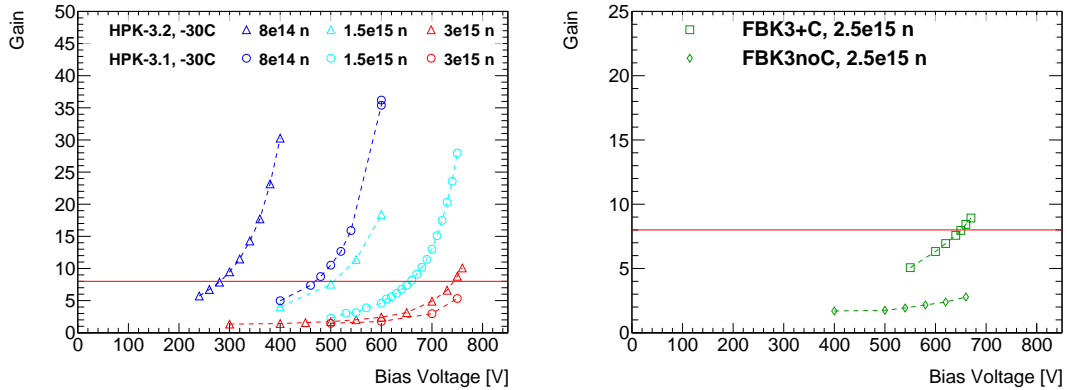


Figure 3: Gain as a function of bias voltage for HPK-3.1/HPK-3.2 (left) and FBK3+C/FBK3noC (right) sensors. The two plots have different vertical scale.

The time resolution is shown in Fig. 4 for the three types of sensors. For HPK-3.2, the time resolution before irradiation is fairly high for a  $50 \mu\text{m}$  thick LGAD; this effect is due to the excessive gain layer doping. The performance is worse, around 100 ps, when the sensor is operated at cold temperatures because of the lowered breakdown voltage (around 75 V), which is very close to the full depletion voltage (70 V). This behavior is consequence of the high initial doping of the multiplication layer, which leads to a breakdown voltage below the minimum voltage needed to obtain a saturated e/h drift velocity; for this reason the doping of future HPK-3.2 productions will be tuned to provide a good balance between operation before irradiation and radiation hardness. The performance improves rapidly with acceptor removal, after slight radiation damage, at the fluence of  $4 \times 10^{14} \text{ n}_{\text{eq}}/\text{cm}^2$  the sensor can reach a time resolution of 30 ps. At the fluence of  $3 \times 10^{15} \text{ n}_{\text{eq}}/\text{cm}^2$  HPK-3.2 can still reach a time resolution of less than 60 ps. At higher fluences the time resolution is significantly worse.

HPK-3.1 has a better performance than HPK-3.1 before irradiation thanks to the higher operating voltage. It has comparable time resolution to HPK-3.2 for low fluences, and can reach a time resolution around 40 ps up to a fluence of  $1.5 \times 10^{15} \text{ n}_{\text{eq}}/\text{cm}^2$ . For a fluence of  $3 \times 10^{15} \text{ n}_{\text{eq}}/\text{cm}^2$ , however, the time resolution is above 60 ps.

FBK3+C sensors has a slightly higher time resolution than HPK-3.1 and HPK-3.2, about 40 ps at lower fluences. It can reach a time resolution below than 60 ps up to  $3 \times 10^{15} \text{ n}_{\text{eq}}/\text{cm}^2$ . However, similarly to the case of HPK-3.2, at  $4 \times 10^{15} \text{ n}_{\text{eq}}/\text{cm}^2$  the time resolution increases above 60 ps.

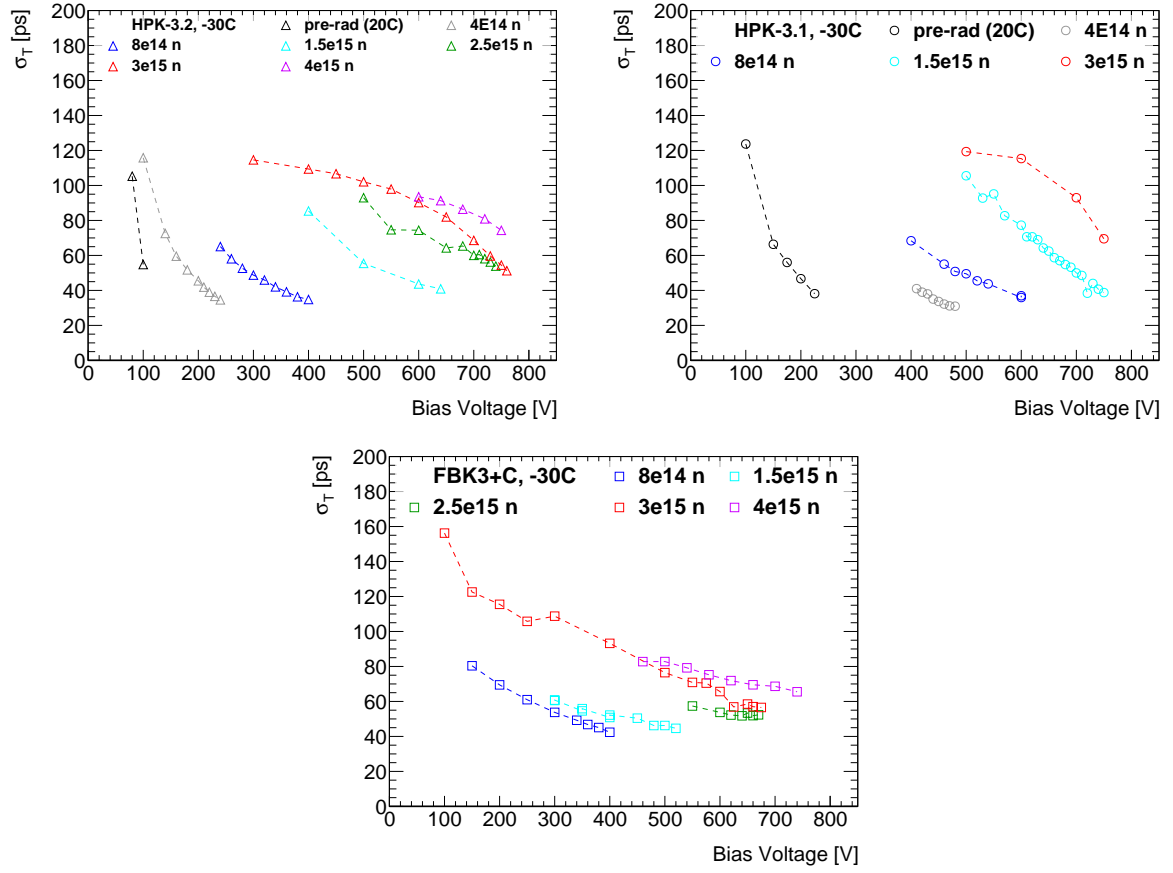


Figure 4: Time resolution as a function of bias voltage for HPK-3.2 (top-left), HPK-3.1 (top-right) and FBK3+C (bottom) sensors.

In Fig. 5 the time resolution is plotted as a function of gain for three types of sensors (HPK-3.2, HPK-3.1 and FBK3+C) each at three fluences ( $8 \times 10^{14} \text{ n}_{\text{eq}}/\text{cm}^2$ ,  $1.5 \times 10^{15} \text{ n}_{\text{eq}}/\text{cm}^2$  and  $3 \times 10^{15} \text{ n}_{\text{eq}}/\text{cm}^2$ ). It can be seen that all curves approximately lie on top of each other, showing a universal dependence of the time resolution with the gain across sensor types, vendors and fluences.

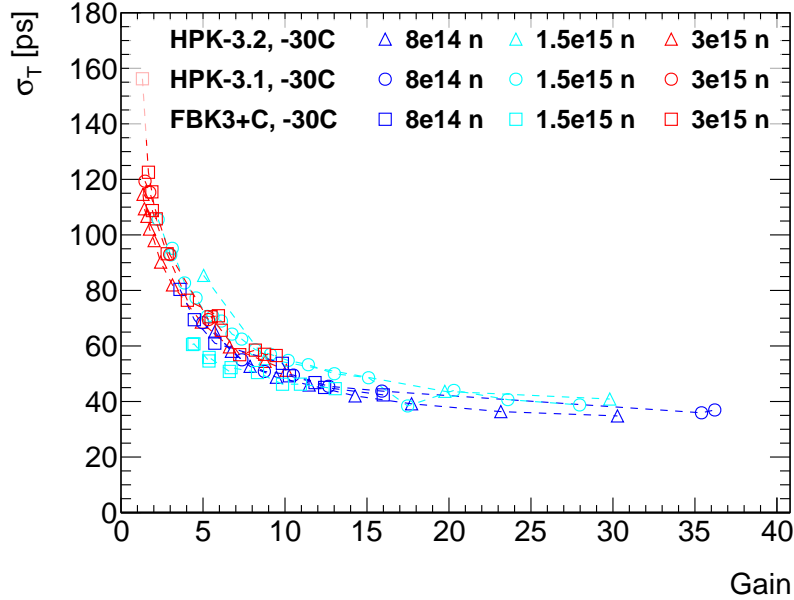


Figure 5: Time resolution as a function of gain for HPK-3.2, HPK-3.1 and FBK3+C at different fluences.

## 6 CV and comparison with collected charge

As mentioned earlier, the doping concentration of the gain layer is proportional to the  $V_{GL}$  extracted from the C-V measurement. The  $1/C^2$  measurement for HPK-3.2, HPK-3.1 and FBK3+C before and after irradiation can be seen in Fig. 6. The effects of acceptor removal in the multiplication layer and the acceptor creation in the bulk are clearly visible by the shortening of  $V_{GL}$  and the changes in the subsequent slope.

As already mentioned, determination of  $V_{GL}$  is performed intersecting the linear fit of the gain layer depletion region with the linear fit of the bulk layer depletion region, an intersection of the two lines is calculated. The extracted value  $V_{GL}$  is the Voltage to deplete the gain layer, the so-called “foot” voltage.

From the  $V_{GL}$  measurement, the fraction of gain layer still active after a given fluence can be extracted. In Fig. 7, the fraction of gain layer is showed as a function of the fluence  $\phi$ . The reduction of the fraction of gain layer can be fitted with the following formula to calculate the  $c$  factor that represent the speed of doping removal:

$$N_D = N_0 \cdot e^{-c\phi} \quad (1)$$

Large differences are seen among the different sensor types: The HPK-3.1 has the largest  $c$ -factor, about a factor 2 larger than HPK-3.2. This shows the advantage of the deeper and narrower doping profile. The FBK3+C has the smallest  $c$  coefficient, about a factor 2 smaller than HPK-3.2: we attribute this effect to the suppression of acceptor removal through the addition of carbon.



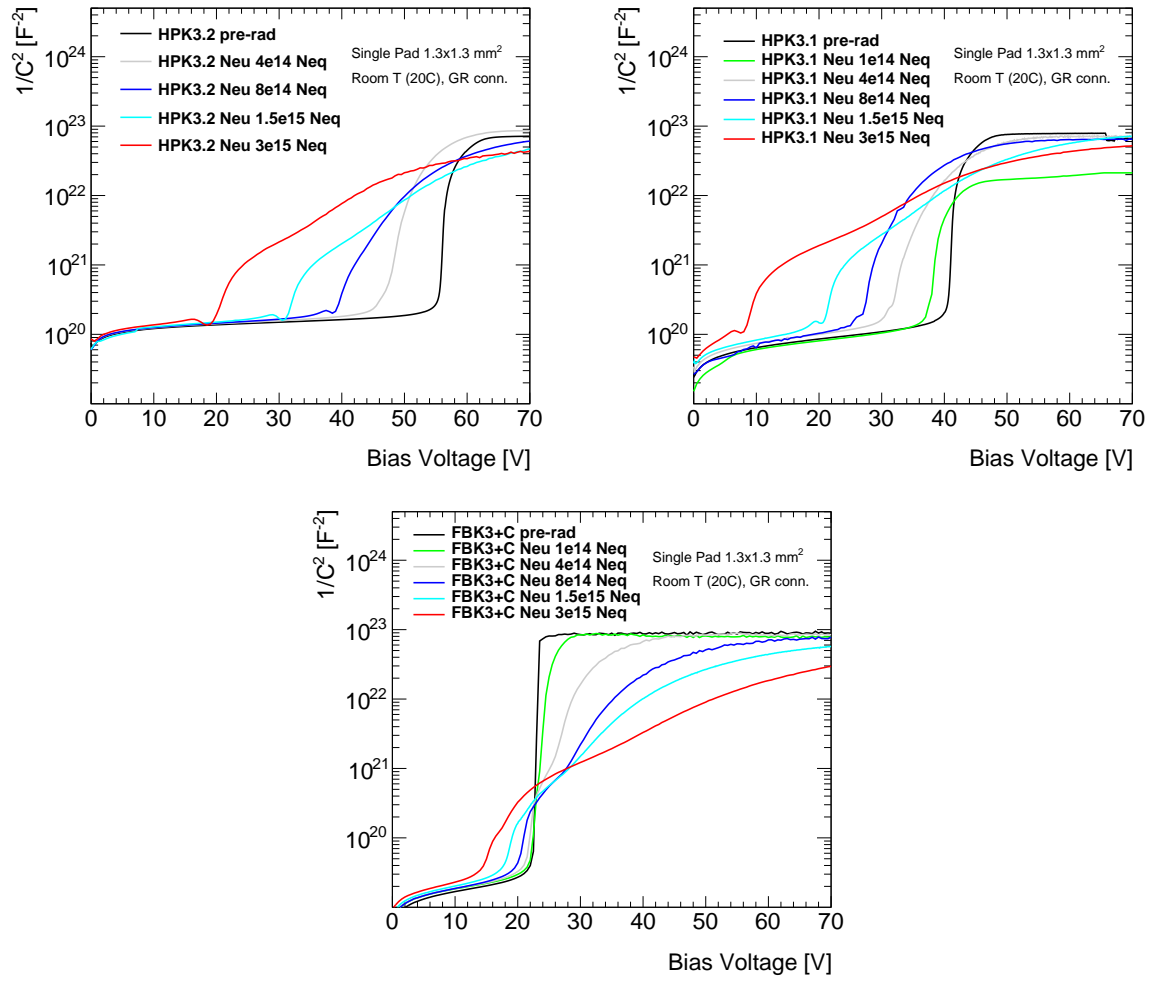


Figure 6: C-V of HPK-3.2 (top-left), HPK-3.1 (top-right) and FBK-C (right) sensors at different radiation level.

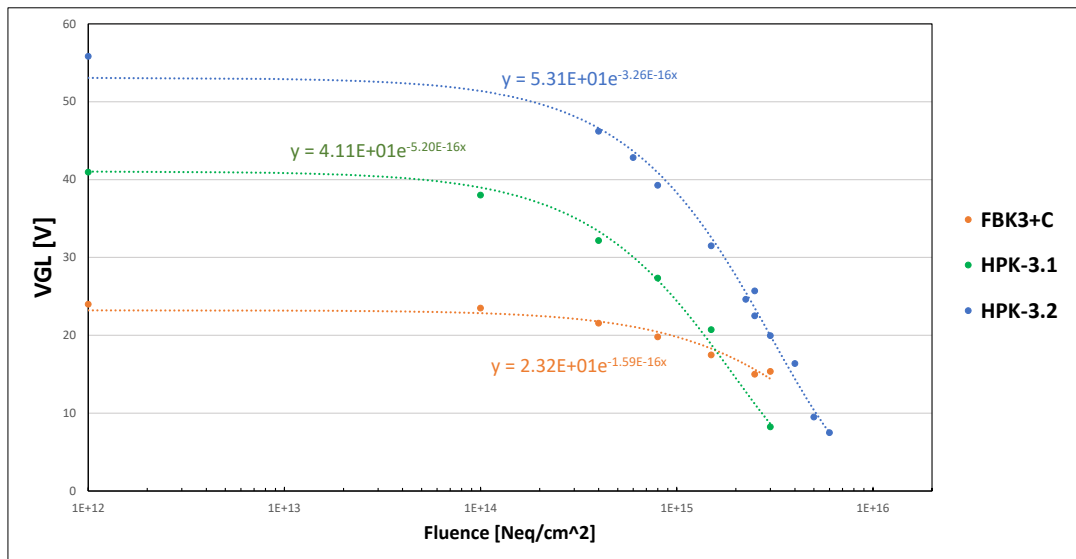


Figure 7: Evolution of  $V_{GL}$  (“foot”) for HPK-3.2, HPK-3.1 and FBK3+C sensors.

The charge collection data (Fig. 2 and Fig. 3) can be characterized by the bias voltage needed to reach a certain gain  $G$ ,  $V(G)$ . In the following analysis, the value to reach a gain of 8 ( $V(G=8)$ ), shown by the red line in Fig. 2 and Fig. 3) is taken into consideration. This value can be correlated with the  $V_{GL}$  value (in Fig. 7) measured in  $1/C^2$  distributions shown in Fig. 6. In the plot in Fig. 8 only sensors that can reach a gain of 8 are taken into consideration. This correlation, seen in Fig. 8, is fitted with a linear function. Both  $V_{GL}$  and  $V(G=8)$  degrade altogether with radiation damage and show a fairly accurate linear correlation. This correlation also means that, after a calibration of the method, the bias required to reach a gain after a certain fluence for a specific type of sensor can be derived from the calculation of  $V_{GL}$  from a  $1/C^2$  measurement.

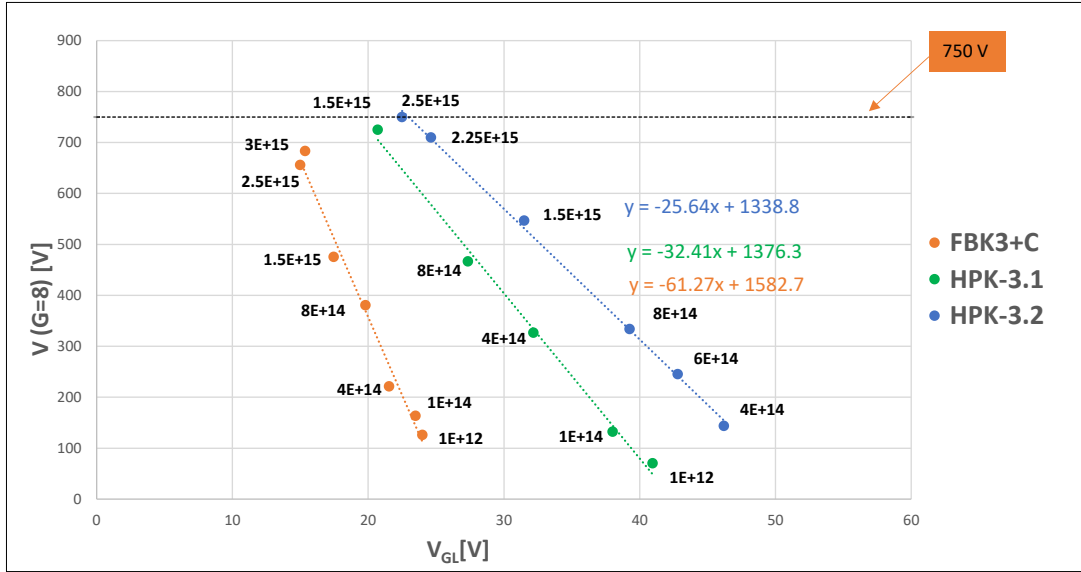


Figure 8: Correlation between  $V_{GL}$  and the bias voltage to acquire gain of 8 ( $V(G=8)$ ). Linear fits are shown in the plot. Results are for three sensors from pre-rad (represented by  $1 \times 10^{12} \text{ n}_{eq}/\text{cm}^2$ ) up to  $3 \times 10^{15} \text{ n}_{eq}/\text{cm}^2$ . Only sensors that can reach a gain of 8 are taken into consideration. The black horizontal dashed line represents 750 V which is the maximum safe voltage for 50  $\mu\text{m}$  thick sensors.

## 7 Review of fluence uncertainty at JSI

Several type of sensors were irradiated to the same fluence at JSI Ljubljana. After sensors testing, a large spread of performance among identical sensors irradiated to what was nominally the same fluence was found. As an example, Fig. 9 (left) shows the gainbias curves for 7 HPK-3.2 sensors after a nominal neutron fluence of  $1.5 \times 10^{15} \text{ n}_{eq}/\text{cm}^2$ . The variation in performance is evident: choosing the value  $V(G=8)$  as representative of the variation the spread in voltage is found to be of the order of 10%. The correlation of the  $V(G=8)$  value with  $V_{GL}$  from  $1/C^2$  (Fig. 10) show a very linear behavior: this is a confirmation that the gain layer of the sensors tested is actually different and performance spread across the sensors is real, caused by different degrees of acceptor removal.

A correction can be applied to the charge collection curves by using the  $V_{GL}$  results from  $1/C^2$  in the following manner: as first step the median value of  $V_{GL}^M$  is calculated, this value is considered to be close to the sensor performance at the actual nominal fluence. Afterwards the shift between the  $V_{GL}$ s and the median  $V_{GL}^M$  is evaluated and correction factors are calculated for the  $V_{bias}$  in the charge collection distributions from the linear correlation in Fig. 10. After this correction, the performance of the sensors match within a few percent (Fig. 9, right) equivalently

to the spread these sensors had before irradiation.

The 10% spread calculated from in Fig. 9 (left) is actually very close to the uncertainty value quoted by the JSI irradiation facility on the fluence. The conclusion of this study is the confirmation that the sensor performance spread seen after irradiation is caused by the uncertainty on the fluence and not by reason intrinsic to the sensor type itself.

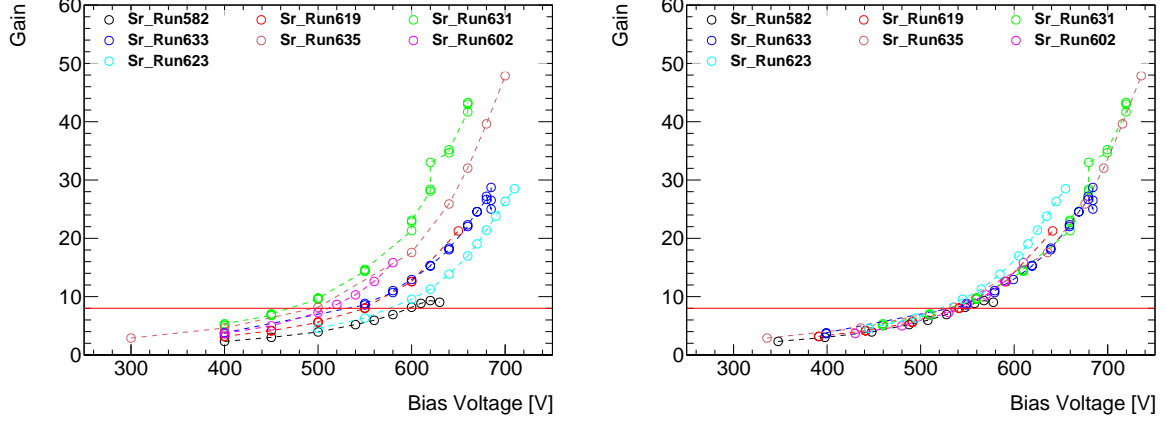


Figure 9: Left: Difference in charge collection curves for several HPK-3.2 sensors all irradiated at a nominal fluence of  $1.5 \times 10^{15} \text{ n}_{\text{eq}}/\text{cm}^2$ . Different Run number represent different HPK-3.2 sensors.  $V(G=8)$  has roughly a 10% variation. Right: Same charge collection after applying a correction based on the  $V_{GL}$  in Fig. 10.  $V(G=8)$  variation is around 1% as was the case for sensors of the same type before irradiation.

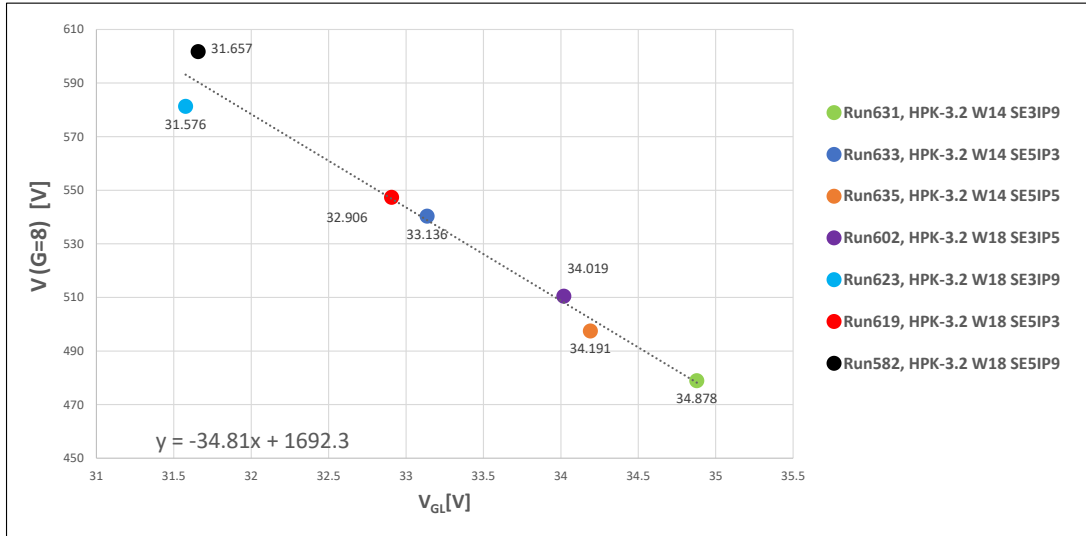


Figure 10: Correlation between  $V_{bias}$  to achieve gain 8 and  $V_{GL}$  (“foot”).

## 8 Conclusions

The performance before and after irradiation of 2 types of HPK and 2 types of FBK sensors have been reviewed. The sensors have been characterized electrically with I-V and C-V curves. From the C-V curves, an indication of the doping concentration and deepness of the gain layer is extracted using the “foot” or  $V_{GL}$ . The study of charge collection has been done using the Sr-90  $\beta$ -telescope setup at SCIPP (Santa Cruz Institute for Particle Physics), University of California Santa Cruz. The following statements can be made from Fig. 2, Fig. 3 and Fig. 4:

- HPK-3.1 shows acceptable radiation hardness up to a neutron fluence of  $1.5 \times 10^{15} \text{ n}_{\text{eq}}/\text{cm}^2$
- The very deep and thin gain layer of HPK-3.2 results in good radiation hardness up to a neutron fluence of  $3 \times 10^{15} \text{ n}_{\text{eq}}/\text{cm}^2$ , however the doping concentration needs to be tuned for optimal operation before irradiation.
- FBK sensors with Carbon (FBK3+C) implantation show exceptional radiation hardness compared to the same kind of sensors with no Carbon (FBK3noC) as seen in Fig. 3 (right).
- HPK-3.2 and FBK3+C both show reasonable performance up to  $3 \times 10^{15} \text{ n}_{\text{eq}}/\text{cm}^2$ , however none of the presented types of sensors is radiation hard up to  $4 \times 10^{15} \text{ n}_{\text{eq}}/\text{cm}^2$ .
- Since the two technologies (Carbon in FBK3+C and deep gain layer in HPK-3.2) are independent from each other, a combination of a deep narrow gain layer with carbon can be expected to show significantly better radiation hardness than either alone.

Further general conclusions:

- The correlation between the time resolution and the gain shown in Fig. 5 is independent from the sensor type (with a similar thickness) and from the fluence.
- The depletion voltage of the gain layer ( $V_{GL}$ ) and the voltage to reach a gain of 8 V ( $G=8$ ) are linearly correlated.
- The correlation shows that is possible, after careful calibration, to foresee the performance of LGADs after irradiation purely from a C-V scan.
- This technique can also be used to evaluate the fluence uncertainty of an irradiation facility.

## 9 Acknowledgements

This work was supported by the United States Department of Energy, grant DE-FG02-04ER41286, and partially performed within the CERN RD50 collaboration. Part of this work has been financed by the European Union’s Horizon 2020 Research and Innovation funding program, under Grant Agreement no. 654168 (AIDA-2020) and Grant Agreement no. 669529 (ERC UFSD669529), and by the Italian Ministero degli Affari Esteri and INFN Gruppo V.

## References

- [1] G. Pellegrini et al., *Technology developments and first measurements of Low Gain Avalanche Detectors (LGAD) for high energy physics applications*, *Nucl. Instrum. Meth.* **A765** (2014) 12 – 16.
- [2] M. Carulla et al., *First 50  $\mu\text{m}$  thick LGAD fabrication at CNM, 28th RD50 Workshop, Torino, Italy, June 7th 2016*, .
- [3] H. F. W. Sadrozinski et al., *Ultra-fast silicon detectors (UFSD)*, *Nucl. Instrum. Meth.* **A831** (2016) 18–23.
- [4] RD50 collaboration, “<https://rd50.web.cern.ch/rd50>.”
- [5] H. Sadrozinski, A. Seiden and N. Cartiglia, *4-dimensional tracking with ultra-fast silicon detectors, Reports on Progress in Physics* (2017) , [[1704.08666](#)].
- [6] HL-LHC, “<http://dx.doi.org/10.5170/CERN-2015-005>.”

- [7] ATLAS collaboration, *Technical Proposal: A High-Granularity Timing Detector for the ATLAS Phase-II Upgrade* <http://cds.cern.ch/record/2623663>, Tech. Rep. CERN-LHCC-2018-023. LHCC-P-012, CERN, Geneva, Jun, 2018.
- [8] CMS collaboration, *A MIP Timing Detector for the CMS Phase-2 Upgrade*, Tech. Rep. CERN-LHCC-2019-003. CMS-TDR-020, CERN, Geneva, Mar, 2019.
- [9] F. Cenna et al., *Weightfield2: A fast simulator for silicon and diamond solid state detector*, *Nucl. Instrum. Meth.* **A796** (2015) 149–153.
- [10] S. M. Mazza et al., *Properties of FBK UFSDs after neutron and proton irradiation up to  $6 \times 10^{15}$  neq/cm<sup>2</sup>*, [1804.05449](#).
- [11] M. Ferrero et al., *Radiation resistant LGAD design*, *Nucl. Instrum. Meth.* **A919** (2019) 16–26, [[1802.01745](#)].
- [12] Y. Zhao et al., *Comparison of 35 and 50  $\mu$ m thin hpk ufsd after neutron irradiation up to  $6 \times 10^{15}$  neq/cm<sup>2</sup>*, [1803.02690](#).
- [13] Z. Galloway et al., *Properties of HPK UFSD after neutron irradiation up to  $6 \times 10^{15}$  n/cm<sup>2</sup>*, submitted to *NIM A* (2017) , [[1707.04961](#)].
- [14] HGTD TEST BEAM GROUP collaboration, L. Masetti et al., *Beam test measurements of low gain avalanche detector single pads and arrays for the atlas high granularity timing detector, to be submitted to JINST* (2018) , [[1804.00622](#)].
- [15] G. Kramberger et al., *Radiation effects in low gain avalanche detectors after hadron irradiations*, *JINST* **10** (2015) P07006.
- [16] Snoj, G. Zerovnik and A. Trkov, *Computational analysis of irradiation facilities at the JSI TRIGA reactor*, *Appl. Radiat. Isot.* **70** (2012) 483. .